J|A|C|S ARTICLES

Published on Web 03/12/2009

# Parameters Influencing the Efficiency of Electron Injection in Dye-Sensitized Solar Cells

Sara E. Koops, Brian C. O'Regan, Piers R. F. Barnes, and James R. Durrant*

*Department of Chemistry, Imperial College London, Exhibition Road, London SW7 2AZ, U.K.*

Received November 28, 2008; E-mail: j.durrant@imperial.ac.uk

***Abstract:*** In this paper we focus upon the electron injection dynamics in complete nanocrystalline titanium dioxide dye-sensitized solar cells (DSSCs) employing the ruthenium bipyridyl sensitizer dye N719. Electron injection dynamics and quantum yields are studied by time-resolved single photon counting, and the results are correlated with device performance. In typical DSSC devices, electron injection kinetics were found to proceed from the N719 triplet state with a half-time of 200 ± 60 ps and quantum yield of 84 ± 5%. We find that these injection dynamics are independent of presence of iodide/triiodide redox couple and of the pH of the peptization step used in the synthesis of the $TiO_2$ nanoparticles. They are furthermore found to be only weakly dependent upon the application of electrical bias to the device. In contrast, we find these dynamics to be strongly dependent upon the concentration of *tert*-butylpyridine (tBP) and lithium cations in the electrolyte. This dependence is correlated with shifts of the $TiO_2$ conduction band energetics as a function of tBP and $Li^+$ concentration, from which we conclude that a 100 meV shift in band edge results in an approximately 2-fold retardation of injection dynamics. We find that the electron injection quantum yield determined from these transient emission data as a function of tBP and $Li^+$ concentration shows a linear correlation with device short circuit density $J_{sc}$. We thus conclude that the relative energetics of the dye excited state versus the titanium dioxide acceptor state is a key determinant of the dynamics of electron injection in DSSC, and that variations in these energetics, and therefore in the kinetics and efficiency of electron injection, impact directly upon device photovoltaic efficiency. Finally, we discuss these results in terms of singlet versus triplet electron injection pathways and the concept of minimization of kinetic redundancy.

## Introduction

Dye-sensitized solar cells (DSSCs) are a potentially lower cost alternative to inorganic silicon-based photovoltaics. DSSCs based on Ru-bipyridyl dyes adsorbed to nanocrystalline titania ($TiO_2$) electrodes in combination with iodide/triiodide redox-based electrolytes have reached efficiencies of >10%.[1] The function of such devices is based upon light-induced charge-transfer processes at the metal oxide/dye/electrolyte interface, and as such the kinetics of these processes can be expected to be key determinants of device performance. The primary charge separation step in DSSCs comprises electron injection from the dye excited state into the $TiO_2$ conduction band (CB). Extensive studies of this electron injection process in $TiO_2$/Ru-bipyridyl dye films coated in inert solvent have shown subpicosecond injection dynamics,[2−5] orders of magnitude faster than the competing process of excited state decay to ground. As such, electron injection has not generally been considered to be a key factor limiting device performance, with most studies of device optimization focusing upon optimizing the light absorption and electron collection aspects of device function.[6] However, we have recently reported an ultrafast transient absorption study of electron injection in a complete DSSC. In contrast to the film studies, we observed a much slower electron injection half-time of ∼150 ps in these devices, slow enough for kinetic competition between electron injection and excited state decay to ground potentially to have a significant impact upon device performance. The slower dynamics in the complete DSSC were attributed to the presence of additives typically added to the device electrolyte to improve photovoltaic performance.[7,8] This observation has motivated us to undertake a detailed study of the parameters influencing electron injection kinetics and yields in complete DSSCs, and thus to quantify the influence of electron injection efficiency upon device performance, as we report herein.

There have been extensive reviews of photoinduced electron transfer processes in Ru-bipyridyl-sensitized $TiO_2$ films in the absence of redox electrolyte.[3,9−13] Commonly ultrafast tech-

(1) Grätzel, M. *Prog. Photovoltaics* **2006**, *14*, 429–442.
(2) Asbury, J. B.; Ellingson, R. J.; Ghosh, H. N.; Ferrere, S.; Nozik, A. J.; Lian, T. Q. *J. Phys. Chem. B* **1999**, *103*, 3110–3119.
(3) Ramakrishna, G.; Jose, D. A.; Kumar, D. K.; Das, A.; Palit, D. K.; Ghosh, H. N. *J. Phys. Chem. B* **2005**, *109*, 15445–15453.
(4) Kuang, D. B.; Ito, S.; Wenger, B.; Klein, C.; Moser, J. E.; Humphry-Baker, R.; Zakeeruddin, S. M.; Grätzel, M. *J. Am. Chem. Soc.* **2006**, *128*, 4146–4154.
(5) Benko, G.; Kallioinen, J.; Korppi-Tommola, J. E. I.; Yartsev, A. P.; Sundstrom, V. *J. Am. Chem. Soc.* **2002**, *124*, 489–493.
(6) Nazeeruddin, M. K.; Wang, Q.; Cevey, L.; Aranyos, V.; Liska, P.; Figgemeier, E.; Klein, C.; Hirata, N.; Koops, S.; Haque, S. A.; Durrant, J. R.; Hagfeldt, A.; Lever, A. B. P.; Grätzel, M. *Inorg. Chem.* **2006**, *45*, 787–797.
(7) Kelly, C. A.; Farzad, F.; Thompson, D. W.; Stipkala, J. M.; Meyer, G. J. *Langmuir* **1999**, *15*, 7047–7054.
(8) Haque, S. A.; Palomares, E.; Cho, B. M.; Green, A. N. M.; Hirata, N.; Klug, D. R.; Durrant, J. R. *J. Am. Chem. Soc.* **2005**, *127*, 3456–3462.



**10.1021/ja8091278 CCC: $40.75** 

niques such as femtosecond transient absorption spectroscopy are used to determine the kinetics of the electron injection process through absorption changes associated with the formation of the dye cation and/or injected electron.[11] Such studies have shown subpicosecond injection processes occurring from the singlet excited state,[2−5] which can compete with intramolecular relaxation within this state.[10,14] Additionally, strong spin−orbit coupling from the ruthenium heavy atom center accelerates intersystem crossing to ∼100 fs,[15] resulting in an additional injection mechanism proceeding via the lower energy triplet excited state and occurring on the picosecond time scale (typically tens of picoseconds), often resulting in biphasic injection kinetics. In these model system studies, the kinetics of electron injection, and the proportion of singlet versus triplet injection, have been studied as a function of excitation wavelength,[10,16−18] solvent choice,[19,20] pH environment,[18,21] inclusion of cationic potential determining ions,[7,22] $TiO_2$ Fermi level,[23,24] and bridging components positioned between the dye and the empty accepting orbitals on the $TiO_2$ surface,[25,26] leading to a detailed understanding of the injection process. In terms of their relevance to device performance, the overall conclusion of these model system studies has typically been that electron injection from such ruthenium bipyridyl sensitizer dyes into $TiO_2$ photoelectrodes is fast relative to excited state decay to ground, and therefore that the efficiency of electron injection is unlikely to be a critical determinant of device performance.

In parallel with these ultrafast studies of electron injection, there have been extensive studies focusing on the optimization of the power conversion efficiency of DSSCs. Relatively few of these studies have considered directly the relevance of the electron injection process in influencing device photovoltaic performance. Of particular note, structure−function studies of a series of organic dyes have highlighted the need for the dye excited state to be sufficiently high in energy to allow injection to occur. Dyes which did not fulfill this requirement were observed to have lower photocurrents.[27−29] Furthermore, improved currents in DSSCs based on the Ru black dye have also been reported to be effected by improved injection performance.[30] Similarly, dye aggregation has been suggested to reduce the efficiency of electron injection for some sensitizer dyes, thereby reducing device performance.[31] Of particular relevance to this paper, studies to optimize device performance have frequently employed electrolyte additives, such as *tert*-butylpyridine (tBP) and $Li^+$, to enhance device performance. The influence of these additives on device performance has been generally attributed to their influence on the $TiO_2$ surface charge, and therefore CB edge. In model systems studies, such additives have been shown to influence electron injection dynamics by modulating the relative energetics of the dye excited state versus the $TiO_2$ CB.[22,24,32] However the influence of such additives upon the efficiency of electron injection in complete DSSCs, and their correlation with device performance, have received only limited attention to date.[7,8,33] This gap arises partly from the difficulty of measuring injection in complete devices using femtosecond transient absorption instruments. As a consequence, DSSC device optimization studies to date typically have not focused on electron injection dynamics as being a significant factor determining device performance.

Scheme 1 shows, to scale, the structure of the active environment in the operating DSSC, illustrating the chemical complexity of the pores of a DSSC in the presence of a typical electrolyte, and thus emphasizing the importance of complete device studies of injection dynamics as opposed to model system studies of dye-sensitized films covered in inert solvent. Our recent observation that electron injection dynamics in a typical complete DSSCs are on the 100 ps time scale,[8] and therefore from the dye triplet state, opens up the potential to measure these injection kinetics in DSSCs not only by ultrafast pump/probe techniques such as transient absorption spectroscopy, but also with single pulse techniques such as time-correlated single photon counting (TCSPC).[34] This greatly simplifies the experimental measurement procedure, allowing, for example, the use of much lower excitation densities, thereby avoiding problems of charge accumulation which have complicated experimental pump/probe studies of complete devices.[8] By using non-injecting control samples (employing $ZrO_2$ films) and matched densities of absorbed photons, we have shown that it is possible to use TCSPC to measure electron injection dynamics in dye-sensitized films with a time resolution of ∼60 ps.[34]

As illustrated in Scheme 1, the $TiO_2$/dye/electrolyte interface exhibits a considerable chemical complexity. In this report, we employ TCSPC measurements to study electron injection in


(9) Thorsmolle, V. K.; Wenger, B.; Teuscher, J.; Bauer, C.; Moser, J. E. *Chimia* **2007**, *61*, 631–634.
(10) Islam, A.; Hara, K.; Singh, L. P.; Katoh, R.; Yanagida, M.; Murata, S.; Takahashi, Y.; Sugihara, H.; Arakawa, H. *Chem. Lett.* **2000**, *490*, 491.
(11) Anderson, N. A.; Lian, T. Q. *Annu. Rev. Phys. Chem.* **2005**, *56*, 491–519.
(12) Ellingson, R. J.; Asbury, J. B.; Ferrere, S.; Ghosh, H. N.; Sprague, J. R.; Lian, T. Q.; Nozik, A. J. *J. Phys. Chem. B* **1998**, *102*, 6455–6458.
(13) Watson, D. F.; Meyer, G. J. *Annu. Rev. Phys. Chem.* **2005**, *56*, 119–156.
(14) Asbury, J. B.; Hao, E.; Wang, Y. Q.; Ghosh, H. N.; Lian, T. Q. *J. Phys. Chem. B* **2001**, *105*, 4545–4557.
(15) Kallioinen, J.; Benko, G.; Sundstrom, V.; Korppi-Tommola, J. E. I.; Yartsev, A. P. *J. Phys. Chem. B* **2002**, *106*, 4396–4404.
(16) Bruggemann, B.; Organero, J. A.; Pascher, T.; Pullerits, T.; Yartsev, A. *Phys. Rev. Lett.* **2006**, 97.
(17) Liu, F.; Meyer, G. J. *Inorg. Chem.* **2003**, *42*, 7351–7353.
(18) Asbury, J. B.; Anderson, N. A.; Hao, E. C.; Ai, X.; Lian, T. Q. *J. Phys. Chem. B* **2003**, *107*, 7376–7386.
(19) She, C. X.; Guo, J. C.; Lian, T. Q. *J. Phys. Chem. B* **2007**, *111*, 6903–6912.
(20) Pollard, J. A.; Zhang, D. S.; Downing, J. A.; Knorr, F. J.; McHale, J. L. *J. Phys. Chem. A* **2005**, *109*, 11443–11452.
(21) Tachibana, Y.; Nazeeruddin, M. K.; Grätzel, M.; Klug, D. R.; Durrant, J. R. *Chem. Phys.* **2002**, *285*, 127–132.
(22) Watson, D. F.; Meyer, G. J. *Coord. Chem. Rev.* **2004**, *248*, 1391–1406.
(23) Tachibana, Y.; Haque, S. A.; Mercer, I. P.; Moser, J. E.; Klug, D. R.; Durrant, J. R. *J. Phys. Chem. B* **2001**, *105*, 7424–7431.
(24) Kuciauskas, D.; Monat, J. E.; Villahermosa, R.; Gray, H. B.; Lewis, N. S.; McCusker, J. K. *J. Phys. Chem. B* **2002**, *106*, 9347–9358.
(25) Asbury, J. B.; Hao, E. C.; Wang, Y. Q.; Lian, T. Q. *J. Phys. Chem. B* **2000**, *104*, 11957–11964.
(26) Houamer-Rassin, C.; Chaignon, F.; She, C.; Stockwell, D.; Blart, E.; Buvat, P.; Lian, T.; Odobel, F. *J. Photochem. Photobiol. A: Chemistry* **2007**, *192*, 56–65.
(27) Hara, K.; Wang, Z. S.; Sato, T.; Furube, A.; Katoh, R.; Sugihara, H.; Dan-Oh, Y.; Kasada, C.; Shinpo, A.; Suga, S. *J. Phys. Chem. B* **2005**, *109*, 15476–15482.
(28) Zhang, X.; Zhang, J. J.; Xia, Y. Y. *J. Photochem. Photobiol. A: Chemistry* **2008**, *194*, 167–172.
(29) Hara, K.; Sato, T.; Katoh, R.; Furube, A.; Ohga, Y.; Shinpo, A.; Suga, S.; Sayama, K.; Sugihara, H.; Arakawa, H. *J. Phys. Chem. B* **2003**, *107*, 597–606.
(30) Wang, Z. S.; Yamaguchi, T.; Sugihara, H.; Arakawa, H. *Langmuir* **2005**, *21*, 4272–4276.
(31) Wenger, B.; Grätzel, M.; Moser, J. E. *J. Am. Chem. Soc.* **2005**, *127*, 12150–12151.
(32) Katoh, R.; Furube, A.; Kasuya, M.; Fuke, N.; Koide, N.; Han, L. *J. Mater. Chem.* **2007**, *17*, 3190–3196.
(33) Haque, S. A.; Tachibana, Y.; Willis, R. L.; Moser, J. E.; Grätzel, M.; Klug, D. R.; Durrant, J. R. *J. Phys. Chem. B* **2000**, *104*, 538–547.
(34) Koops, S. E.; Durrant, J. R. *Inorg. Chim. Acta* **2008**, *361*, 663–670.

***Scheme 1.*** Schematic of the Chemical Composition of a Typical Pore in a Complete DSSC Filled with Redox Electrolyte[a]

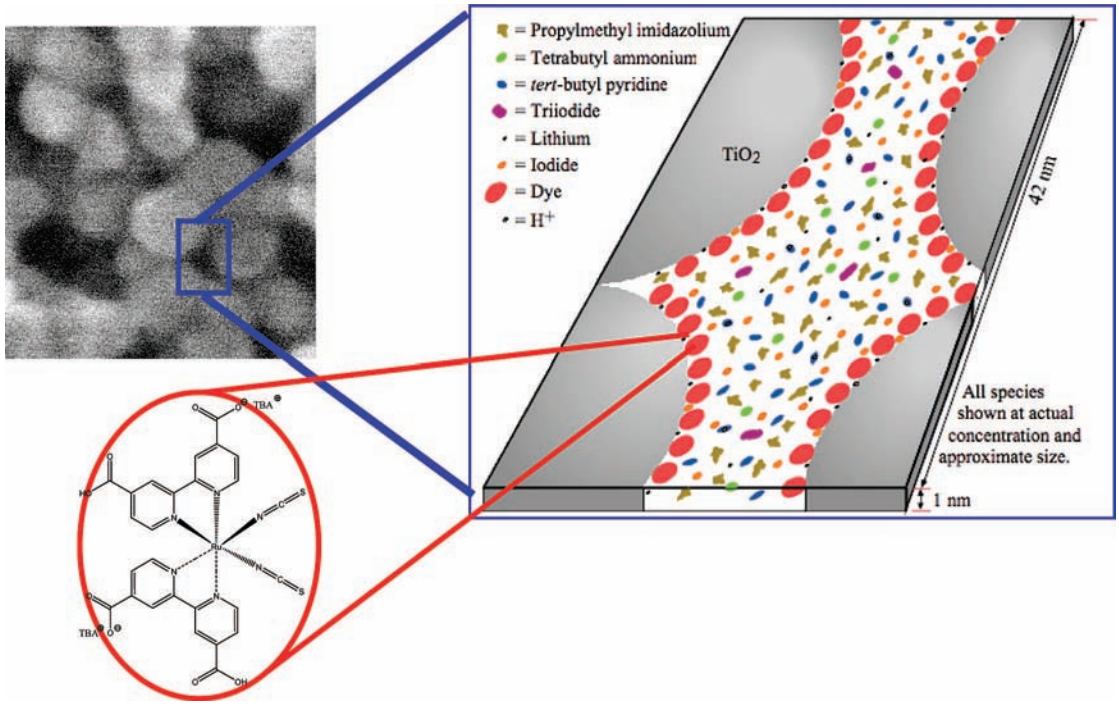


[a] All components are drawn approximately to scale, neglecting molecular interactions. Also shown are a HRSEM image of such a pore and the molecular structure of the N719 sensitizer dye. This illustration neglects intermolecular complexation which is likely to further complicate the chemical composition of the pores.

complete, functioning DSSCs under different operating environments as a function of the chemical composition of this interface. We then quantitatively correlate these dynamics with device performance. We employ devices based upon the widely used N719 sensitizer dye, the di-tetrabutylammonium salt of the commonly used $[RuL_2(NCS)_2]$ (L = 4,4′-dicarboxy-2,2′-bipyridyl) dye. We address the influence of a range of parameters upon electron injection, including the $TiO_2$ film synthesis, electrolyte additives including $Li^+$ ions, tBP, and the $I^-/I_2$ couple, and applied bias. These studies enable us both to elucidate key parameters influencing injection efficiency in complete DSSCs and to relate these observations directly to device performance.

## Experimental Section

Transparent conducting oxide-coated glass substrates were obtained from Hartford Glass Co. Inc. (15 Ω $cm^{-2}$ F-doped $SnO_2$). The $TiO_2$ paste, consisting of 10−15 nm-sized anatase particles, was prepared via a sol−gel route, as described previously. [35] The peptization steps employed either 0.1 M nitric acid (acid film) or 0.1 M ammonia (basic film) to ensure electrostatic stabilization of the deagglomerated $TiO_2$ particles. [35] All solvents and additives were purchased from Aldrich and were HPLC grade. The dye was purchased from Dyesol and used as received.

**Sample/Device Preparation.** Liquid electrolyte devices were fabricated as described previously,[8] using relatively thin (4 $\mu$m) and non-scattering $TiO_2$ films, to optimize compatibility with TCSPC experiments. Briefly, after F-doped $SnO_2$ glass substrates were cleaned with acetone, methanol, and Helmanex, a nanocrystalline, mesoporous $TiO_2$ film (thickness 4 $\mu$m) was fabricated via doctor-blading the $TiO_2$ paste, followed by sintering at 450 °C. N719 was adsorbed to the $TiO_2$ film by immersion overnight in a 0.3 mM solution in acetonitrile:*tert*-butanol (1:1) and subsequently carefully rinsed with acetonitrile. Sensitizing solutions were sonicated prior to film immersion to avoid the presence of dye aggregates in the sensitizing solution. Devices employed a "standard" electrolyte A, consisting of 0.6 M tetrabutylammonium iodide, 0.5 M *tert*-butylpyridine, 0.1 M lithium iodide, and 100 mM iodine in 3-methoxypropionitrile, unless otherwise stated. Transparent counter electrodes were prepared by chemically depositing platinum from 0.05 M hexachloroplatanic acid in 2-propanol onto a second slide of conducting glass. Sandwich cells (1 $cm^2$) were then prepared by sealing together the $TiO_2$-coated electrode with the counter electrode using a transparent film of Surlyn 1472 polymer (DuPont Ltd.) at 110 °C. The electrolyte was then introduced through holes drilled in the counter electrode, which were sealed immediately with microscope cover slides and additional strips of Surlyn to avoid leakage.

**Functional Characterization.** Electron injection dynamics were monitored as described previously,[34] using TCSPC, employing a Jobin Yvon IBH Fluorocube laser system. The apparatus employed 467 nm excitation (1 MHz repetition rate, 80 $\mu$W $cm^{-2}$ average intensity, 250 ps fwhm instrument response), with a 695 nm high-pass filter for emission detection. Samples consisted of dye-sensitized electrodes covered in either 3-methoxypropionitrile or the specified electrolyte, or complete DSSCs employing the specified electrolyte. Control, non-injecting samples were fabricated using sensitized $ZrO_2$ nanocrystalline films. $ZrO_2$ exhibits dye-binding properties similar to those of $TiO_2$ but has a CB edge ~1 eV more negative than that of $TiO_2$, thus preventing electron injection from the dye excited state.

Data were collected on optical-density-matched $ZrO_2$/N719 and $TiO_2$/N719 samples for fixed time periods, resulting in matched densities of absorbed photons, and allowing us to compare amplitudes of traces directly. For all scenarios N719 decays on $ZrO_2$ were longer lived and had higher amplitudes than the $TiO_2$ analogues. The loss in emission with the $TiO_2$ samples is assigned to the additional, non-radiative electron injection pathway into the $TiO_2$. This pathway is forbidden in $ZrO_2$ samples because of its higher CB edge.[36]

(35) Barbe, C. J.; Arendse, F.; Comte, P.; Jirousek, M.; Lenzmann, F.; Shklover, V.; Grätzel, M. *J. Am. Ceram. Soc.* **1997**, *80*, 3157–3171.

Device current−voltage characteristics were determined by illuminating with a 150 W xenon lamp (Sciencetech model SS150W solar simulator), equipped with an IR filter (water filter) and an AM1.5 filter (Sciencetech). Beam intensity was calibrated using an externally calibrated silicon photodiode with a spectral response modified to approximately match the absorption profile of the N719 dye. Current and voltage were measured and controlled using a Keithley 2400 source meter. We note that, due to the use of relatively thin and non-scattering $TiO_2$ films (to facilitate transient spectroscopic studies and avoid electron collection limitations on device short circuit current), these devices yielded only modest photocurrent densities. For standard devices, employing electrolyte A, device efficiencies were determined to be ~4%, with a short circuit current density of 11 mA $cm^{-2}$. Device internal quantum efficiencies (or "absorbed photon to current efficiencies") were determined to be ~86%, indicative of efficient electron injection.

**Data Analysis.** All emission decay traces were normalized for number of photons absorbed at the 467 nm excitation wavelength. Data fitting procedures have been described in detail elsewhere.[34] Control data collected on $ZrO_2$ samples were fitted to biexponential decays, as previously. Data collected for $TiO_2$ samples were fitted by the convolution of the Gaussian instrument response function with a single stretched exponential:

$$\text{Int} = A_0\, e^{-(t/\tau)^{\beta}}$$

where $\beta$ is the stretch parameter ($\beta = 1$ corresponding to a monoexponential decay). We have previously shown that this stretched exponential analysis allows us to fit the emission decays with a minimal number of free parameters, and is moreover consistent with a microscopic model of electron injection based on an inhomogeneous distribution of injection energetics.[37] The amplitude $A_0$ of the stretch exponential was set to the deconvoluted amplitude of the control non-injecting ($ZrO_2$) emission trace, and was therefore not a free parameter in analysis of $TiO_2$-based samples. The fits to the $TiO_2$ data thus use only two free fitting parameters ($\tau$ and $\beta$), thereby greatly increasing the reliability and validity of the fitting procedure. This procedure, using the non-injecting control, allows us to take quantitative account of any ultrafast phases of electron injection not resolved by the instrument response, and results in our analyses having an effective time resolution after deconvolution of ~60 ps.

Decay dynamics were quantified by quoting half-times ($t_{50\%}$) for the injection process. This half-time is defined as the time at which the amplitude of the deconvoluted fit decays to half the initial amplitude of the control (non-injecting) data. The $\beta$ values were $0.353 \pm 0.028$ for all samples employing electrolyte A and varied by only 0.02 between zero and maximum applied negative bias. This allowed half-times between samples to be directly compared. In the tBP studies $\beta$ values ranged more significantly from 0.3 to 0.39, and for this reason we have considered the quantum yields of electron injection in tandem with the $t_{50\%}$ values. Injection quantum yields were determined by integration of the emission decays over time, with the lower integrated areas observed for the $TiO_2$ films relative to the $ZrO_2$ control being assigned to electron injection. We note that, due to the non-exponential nature of the emission decay dynamics observed for the $TiO_2$ samples, the calculated injection quantum yields are significantly lower than those obtained from comparison of decay half-times alone.

## Results

Figure 1 shows typical emission decays observed in a complete DSSC using our electrolyte A, and control data collected for a $ZrO_2$ control cell. The emission decay traces for the control $ZrO_2$ samples typically showed $t_{50\%} \approx 10$ ns, consistent with previous studies of the decay dynamics of the N719 triplet excited state.[38] In the $TiO_2$-based complete DSSC, this emission is strongly quenched, assigned to quenching of the N719 triplet excited state by electron injection into the $TiO_2$ CB. Analysis of the $TiO_2$ data by a stretched exponential model, and deconvolution of the instrument response, as detailed above, allows us to determine an injection half-time, $t_{50\%}$, of $200 \pm 60$ ps. [34] This half-time is typical of devices employing electrolyte A. These kinetics were found to be independent of dye loadings (for devices corresponding to approximately 10−100% monolayer dye coverages). We note that, in this analysis, the initial amplitude is fixed to the amplitude of the non-injecting sample, reducing the free parameters in this fit to only two, and allowing us to take quantitative account of any ultrafast injection phase(s) not fully resolved by our system's instrument response. This injection half-time is in good agreement with our previous transient absorption studies (collected with a subpicosecond instrument response) which resolved an injection half-time of $150 \pm 50$ ps for analogous DSSCs.[8]

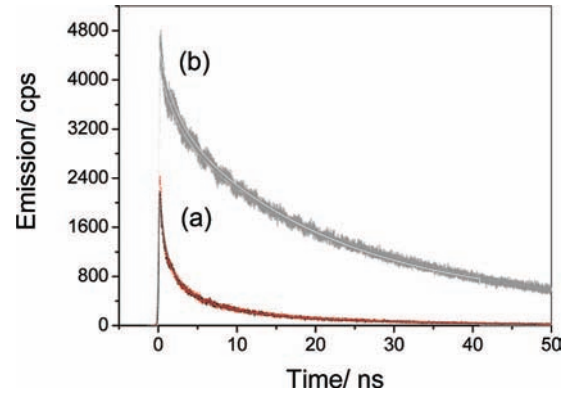


***Figure 1.*** Time-resolved emission decays for (a) N719/$TiO_2$ (black) and (b) N719/$ZrO_2$ (gray) films in electrolyte A. Also shown (a) are the corresponding data collected for an electrolyte omitting the iodide/iodine redox couple (red), which are essentially identical to those observed in the presence of electrolyte A. Smooth lines correspond to fits to the experimental data after convolution with the instrument response.

The dispersive (stretched exponential) nature of the emission decays observed in Figure 1 prevents us from determining the yield of electron injection from measurement of the injection half-time alone. Rather, quantification of the yield of electron injection can be made most easily by comparison of the integrated areas under the emission decays for the $TiO_2$ and $ZrO_2$ samples—with the magnitude of quenching of this emission area observed for the $TiO_2$ samples being taken as a measure of the injection yield. Employing this analysis, we obtain an injection quantum yield of 0.84. We note that this quantum yield is lower than would be expected from considering the half-times alone (150 ps and 10 ns on $TiO_2$ and $ZrO_2$); this lower quantum yield results from the dispersive (stretched exponential) nature of the injection dynamics. This subunity value for the injection quantum yield indicates that, even for this "standard" device, injection efficiency may be limiting device performance.

This measured injection yield was found to be in excellent quantitative agreement with the maximum internal quantum efficiency (or absorbed photon to current efficiency) for these

(36) Kay, A.; Humphrybaker, R.; Grätzel, M. *J. Phys. Chem.* **1994**, *98*, 952–959.

(37) Tachibana, Y.; Rubtsov, I. V.; Montanari, I.; Yoshihara, K.; Klug, D. R.; Durrant, J. R. *J. Photochem. Photobiol. A: Chemistry* **2001**, *142*, 215–220.

(38) We note all sample preparation was undertaken under aerobic conditions; the excited state decay dynamics on $ZrO_2$ may therefore be limited in part.

standard devices, determined under short circuit conditions to be 0.86.[39] It was moreover found to be in good quantitative agreement with analysis of injection efficiency determined from front and back illumination external quantum efficiency data, as we report in detail elsewhere.[39] These observations strongly indicate that, for these "standard" N719 sensitized devices, the internal quantum efficiency for photocurrent generation is limited primarily by the efficiency of electron injection, as we discuss in more detail below.

**Injection Dynamics in the Presence and in the Absence of Redox Couple.** We now turn to consideration of parameters which may influence the observed electron injection dynamics. We consider first the potential influence of the iodide/tri-iodide redox couple in quenching the sensitizer dye excited state. As illustrated in Scheme 1, the redox couple can be expected to have a significant impact upon the chemical environment of the dye/$TiO_2$ interface. Previous studies of analogous ruthenium dyes have indicated that this redox couple can potentially quench the dye triplet excited state by either oxidative or reductive quenching, and that this may be a significant factor influencing DSSC device performance.[40−43]

$$\mathrm{Dye^*} + \mathrm{I_2} \rightarrow \mathrm{Dye^+} + \mathrm{I_2^-} \quad (1)$$

$$\mathrm{Dye^*} + \mathrm{I^-(I_3^-)} \rightarrow \mathrm{Dye^-} + {}^1/_2\mathrm{I_2} \quad (2)$$

To address these issues, we collected data on samples as above but omitting the iodide/iodine redox couple (electrolyte B, with iodide anions replaced by perchlorate). Typical transient emission data are overlaid upon data collected in the presence of the redox couple (electrolyte A) in Figure 1 (electrolyte B, red trace). It is apparent that, for both the $TiO_2$ and $ZrO_2$ control samples, data collected in the presence and in the absence of the redox couple are indistinguishable. It can be concluded that neither oxidative nor reductive quenching of the N719 dye excited state, nor the influence of the redox couple on the $TiO_2$ electron density in the dark, are significant factors influencing electron injection efficiency for N719-sensitized solar cells employing this electrolyte A.

**$TiO_2$ Films Prepared via Acid or Base Peptization.** We turn now to the potential influence of $TiO_2$ film fabrication procedure upon the injection kinetics. Electron injection in dye/$TiO_2$ films has previously been reported to be sensitive to film preparation,[44] while extensive studies have addressed the influence of film preparation upon device performance.[45] One of the main preparatory steps in the $TiO_2$ colloidal film synthesis is the peptization process. Peptization involves electrostatically stabilizing $TiO_2$ film particles by addition of acid ($TiO_{2Acid}$), as employed for "standard" devices studied herein, or base ($TiO_{2Base}$) (Scheme 2).[35] The use of either acid- or base-peptized films has been reported to influence film electron densities and thereby device performance.[45] Furthermore, model system studies of dye/$TiO_2$ electron injection have shown a strong dependence upon ambient pH.[21,46]

***Scheme 2.*** Schematic of $TiO_2$ Particles Following Acid (Positive) or Base (Negative) Peptization


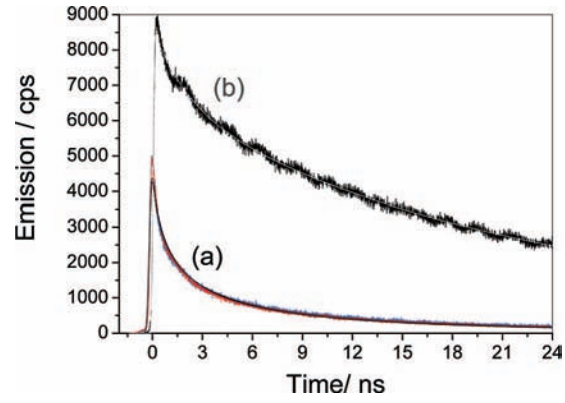


***Figure 2.*** (a) Time-resolved emission decays for N719/$TiO_{2Acid}$ (blue) and N719/$TiO_{2Base}$ (red) films in electrolyte A. Also shown are (b) the corresponding N719/$ZrO_2$ control data and (smooth lines) the convoluted fits to experimental data.

Typical transient emission data of electron injection in either $TiO_{2Acid}$/N719- or $TiO_{2Base}$/N719-sensitized films in electrolyte A are shown in Figure 2. It is apparent that the electron injection dynamics for these two film preparation procedures are indistinguishable. We thus conclude that electron injection in the N719-sensitized solar cells is unaffected by the pH of the initial peptization used in film preparation. We discuss below how to reconcile this observation with device data showing significant differences in device performance.

**Influence of Applied Electrical Bias.** We now consider the effect of electrical bias on electron injection in DSSCs. In model system studies employing three-electrode photoelectrochemical cells, we have shown that the application of an electrical bias of −700 mV relative to Ag/AgCl to N3/$TiO_2$ films (where N3 is the fully protonated analogue of N719) in the presence of a redox-inactive electrolyte retards the injection rate 25-fold (Scheme 3).[23] This retardation was assigned to an increase in electron density within the $TiO_2$ CB, reducing the density of unoccupied states available for electron injection. Solar irradiation of complete DSSCs has also been shown to result in substantial increases in electron density, depending upon irradiation intensity and cell voltage. For example, for the "standard" DSSCs studied herein, charge extraction studies under simulated AM1.5 conditions determined increases in electron density, relative to the dark short circuit conditions, of $\sim 3 \times 10^{17}$ $cm^{-3}$ at short circuit and $\sim 3 \times 10^{18}$ $cm^{-3}$ at open circuit, in good agreement with previous work.[47] This increase

(39) Barnes, P. R. F.; Anderson, A. Y.; Koops, S. E.; Durrant, J. R.; O' Regan, B. C. *J. Phys. Chem. C* **2008**, in press.
(40) Smeigh, A. L.; Katz, J. E.; Brunschwig, B. S.; Lewis, N. S.; McCusker, J. K. *J. Phys. Chem. C* **2008**, *112*, 12065–12068.
(41) Marton, A.; Clark, C. C.; Srinivasan, R.; Freundlich, R. E.; Sarjeant, A. A. N.; Meyer, G. J. *Inorg. Chem.* **2006**, *45*, 362–369.
(42) Wang, P.; Wenger, B.; Humphry-Baker, R.; Moser, J. E.; Teuscher, J.; Kantlehner, W.; Mezger, J.; Stoyanov, E. V.; Zakeeruddin, S. M.; Grätzel, M. *J. Am. Chem. Soc.* **2005**, *127*, 6850–6856.
(43) Clark, C. C.; Marton, A.; Srinivasan, R.; Sarjeant, A. A. N.; Meyer, G. J. *Inorg. Chem.* **2006**, *45*, 4728–4734.
(44) Kallioinen, J.; Benko, G.; Myllyperkio, P.; Khriachtchev, L.; Skarman, B.; Wallenberg, R.; Tuomikoski, M.; Korppi-Tommola, J.; Sundstrom, V.; Yartsev, A. P. *J. Phys. Chem. B* **2004**, *108*, 6365–6373.
(45) Hore, S.; Palomares, E.; Smit, H.; Bakker, N. J.; Comte, P.; Liska, P.; Thampi, K. R.; Kroon, J. M.; Hinsch, A.; Durrant, J. R. *J. Mater. Chem.* **2005**, *15*, 412–418.
(46) Nazeeruddin, M. K.; Humphry-Baker, R.; Liska, P.; Grätzel, M. *J. Phys. Chem. B* **2003**, *107*, 8981–8987.

***Scheme 3.*** Illustration of the Effect of Negative Bias on Electron Injection[a]

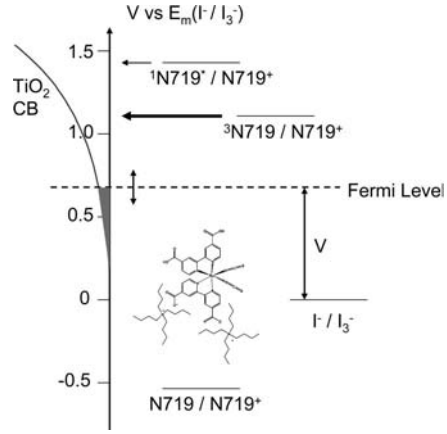


[a] The applied bias, $V$, raises the $TiO_2$ Fermi level relative to the chemical potential of the electrolyte. This results in increasing occupancy of electron acceptor states in the $TiO_2$, illustrated as the shaded area in the exponentially increasing density of CB/trap states.

in electron density, and therefore in $TiO_2$ Fermi level, $E_F$, has been shown to accelerate interfacial charge recombination losses, with a 100 mV increase in $E_F$ typically decreasing the recombination half-time by a factor of 5. It is therefore of interest to consider the influence of applied electrical bias upon the injection dynamics in DSSCs.

Transient emission data were collected for standard N719/$TiO_2$ DSSCs employing electrolyte A under forward bias in the dark for the bias range 0 V (corresponding to short circuit) to −1.07 V (greater than the device $V_{OC}$ under 1 sun, ∼0.76 V). Corresponding charge extraction data indicate that this voltage range corresponds to electron densities up to $6 \times 10^{18}$ $cm^{-3}$, and therefore corresponds to the full range of electron densities present in devices under solar irradiation. Typical data for a device under 0 V (blue) and maximum 1.07 V negative bias (red) are shown in Figure 3.

Control data on the $ZrO_2$ device as a function of applied bias showed, as expected, no dependence upon applied bias. For the $TiO_2$ DSSC, the application of negative bias resulted in a modest increase in electron injection half-time, $t_{50\%}$, from 180 ps at 0 V to 230 ps at −1.07 V, as shown in Figure 3. This effect was fully reversible with variation in applied voltage. Similar, weak but measurable dependence of injection half-times upon applied voltage was observed for all such DSSCs studied. Determination of the electron injection quantum yields (from the integrated emission areas, as detailed above) indicated that the applied bias results in a modest reduction in quantum yield from 0.83 at 0 V to 0.76 at −1.07 V, as illustrated in Figure 3(ii). Quantitative analysis of the origin of bias dependence, and its impact upon device performance, is discussed below.

**Affect of Electrolyte Additives, $Li^+$ and tBP.** We conclude our study by considering the effect of two commonly used electrolyte additives, *tert*-butylpyridine (tBP) and lithium cations ($Li^+$), on electron injection (Scheme 4). Device optimization is commonly achieved by including these electrolyte additives, or analogues, in the cell to modulate the maximum device short circuit current ($J_{SC}$) and maximum open circuit voltage ($V_{OC}$).[8,49−53] tBP and $Li^+$ have been shown to affect both the kinetics and the quantum yield of injection in Ru-bipyridyl-

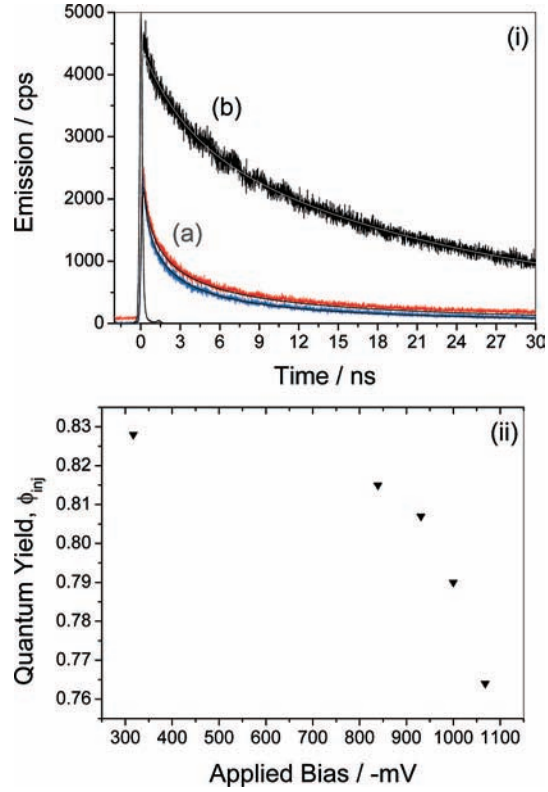


***Figure 3.*** (i) (a) Time-resolved emission decays for N719/$TiO_2$ DSSC employing the electrolyte A under 0 V (blue) and −1.07 V (red) applied bias. (b) Control data for N719/$ZrO_2$ devices. Also shown are stretch-exponential fits to the $TiO_2$ data (smooth lines). (ii) Plot of quantum yield for electron injection, $\phi_{inj}$, determined from emission decays such as those shown in (i) versus applied bias.

***Scheme 4.*** Effect of Commonly Used Electrolyte Additives on the Energetics of the Density of $TiO_2$ Conduction Band Acceptor States[a]

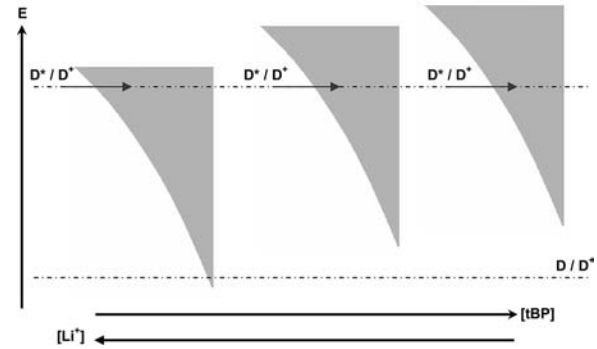


[a] The density of CB/trap states (shaded areas) is represented as an exponential distribution, consistent with previous measurements.[48]

sensitized systems.[7,8,32,54] We extend herein these measurements to complete, functioning devices and quantitatively correlate changes in device $J_{SC}$ and $V_{OC}$ values with modulation of the electron injection process.

Transient emission traces were collected for complete N719/$TiO_2$ DSSCs employing electrolytes based on A but using tBP

(47) O'Regan, B. C.; Durrant, J. R.; Sommeling, P. M.; Bakker, N. J. *J. Phys. Chem. C* **2007**, *111*, 14001–14010.
(48) Durrant, J. R.; Haque, S. A.; Palomares, E. *Coord. Chem. Rev.* **2004**, *248*, 1247–1257.
(49) Kuang, D. B.; Klein, C.; Snaith, H. J.; Moser, J. E.; Humphry-Baker, R.; Comte, P.; Zakeeruddin, S. M.; Grätzel, M. *Nano Lett.* **2006**, *6*, 769–773.
(50) Nakade, S.; Kanzaki, T.; Kubo, W.; Kitamura, T.; Wada, Y.; Yanagida, S. *J. Phys. Chem. B* **2005**, *109*, 3480–3487.

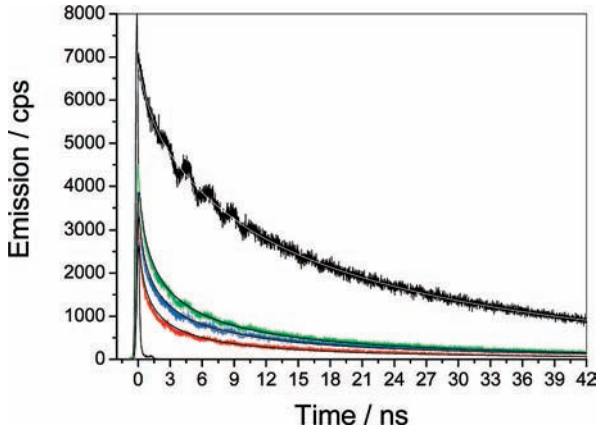


***Figure 4.*** (a) Time-resolved emission decays for N719/$TiO_2$ films in electrolytes employing 0.1 M tBP/0.1 M $Li^+$ (red), 0.2 M tBP/0.1 M $Li^+$ (blue), and 0.2 M tBP/0 M $Li^+$ (green). Also shown are the corresponding N719/$ZrO_2$ control data (black) and (smooth lines) the fits to experimental data.

***Table 1.*** Device and Electron Injection Parameters Measured in Complete Cells Employing Electrolytes with Varying tBP Concentrations with and without the Addition of 0.1M $Li^+$[a]

| [tBP] | [$Li^+$] | $t_{50\%}$/ps | $J_{SC}$/mA cm$^{-2}$ | $V_{OC}$/mV cm$^{-2}$ | $\eta$/% | quantum yield | relative CB energy/V |
|---|---|---|---|---|---|---|---|
| 0 | 0.1 | <60 | 11.28 | 565 | 2.55 | 0.97 | – |
| 0.1 | 0.1 | 70 ± 30 | 10.81 | 621 | 3.35 | 0.87 | 0.47 |
| 0.1 | – | 272 ± 79 | 7.40 | 734 | 3.42 | 0.79 | 0.71 |
| 0.2 | 0.1 | 185 ± 63 | 9.83 | 651 | 3.62 | 0.77 | 0.52 |
| 0.2 | – | 395 ± 96 | 7.32 | 738 | 3.41 | 0.72 | 0.722 |
| 0.5 | 0.1 | 202 ± 71 | 9.55 | 670 | 3.82 | 0.78 | – |
| 0.5 | – | 547 ± 121 | 6.54 | 762 | 3.04 | 0.70 | 0.75 |

[a] All devices use 0.6 M $I^-$/100 mM $I_2$.

and $Li^+$ concentrations varied over the range typically used in DSSC device optimization studies (0−0.1 M $Li^+$, 0−0.5 M tBP). Typical emission data for three different electrolyte compositions are shown in Figure 4.

It is apparent that electrolyte composition has a significant influence upon injection dynamics, with injection half-times ranging from <60 ps for 0.1 M $Li^+$, 0 M tBP to 550 ± 120 ps for 0 M $Li^+$, 0.5 M tBP. Injection half-times and the corresponding device performance data are summarized in Table 1 (we note that devices were fabricated with 4 $\mu$m, non-scattering $TiO_2$ films in order to facilitate TCSPC studies and therefore exhibit only modest absolute current densities due to relatively low light absorption). The variation of device performance with electrolyte composition is in good agreement with previous studies which have shown that more "basic" electrolytes (low $Li^+$, high tBP) reduce $J_{SC}$ but increase $V_{OC}$,[8,49,50,52] with optimum device efficiency being obtained at the "standard" electrolyte composition of 0.1 M $Li^+$, 0.5 M tBP.

Charge extraction measurements[55] were employed to determine the relative $TiO_2$ CB energies for the series of devices studied (with the energies quoted corresponding to the open circuit voltage corresponding to a photoinduced electron density of $10^{18}$ cm$^{-3}$). As expected, the addition of tBP was observed to result in a shift of this density of states to more negative potentials, while addition of $Li^+$ shifted it less negative (toward the redox couple potential). Figure 5 plots the correlation between these relative CB energies and the injection half-time. A reasonable correlation is observed, with a 100 mV shift in CB energetics correlating with a 2-fold increase in injection half-time.

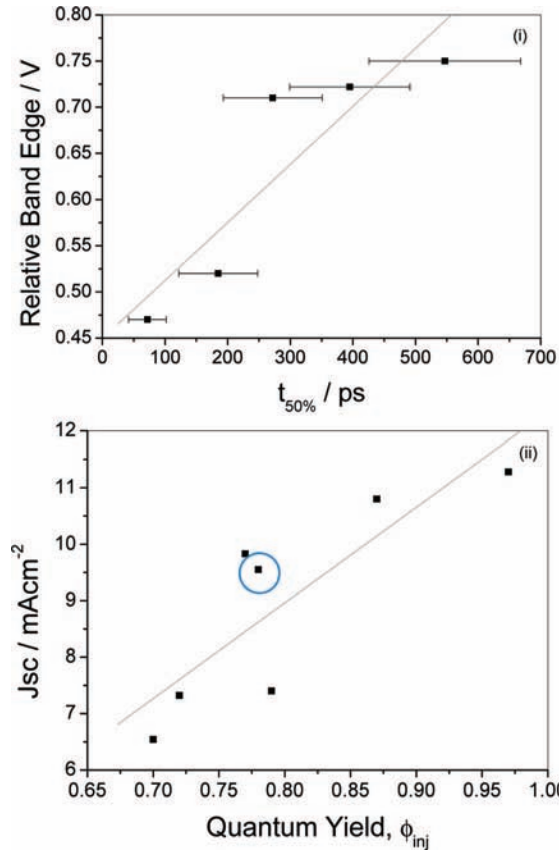


***Figure 5.*** (i) Plot of the electron injection half-time determined from TCSPC data versus an estimate of the relative energies of the $TiO_2$ CB determined from charge extraction data for DSSCs fabricated with different concentrations of $Li^+$ and tBP in the electrolyte. (ii) The corresponding plot of the electron injection yield, $\phi_{inj}$, determined from TCSPC data versus the device short circuit currents measured under 1 sun simulated irradiation. Also shown are the linear best fits in gray. In (ii), the data point corresponding to the highest device efficiency is circled in blue. It is apparent that the device with the fastest injection dynamics, and highest injection yield, does not correspond to the device with the highest overall device efficiency.

We conclude by considering the correlation between injection yield, $\phi_{inj}$, and device photocurrent as a function of electrolyte additives. The electron injection yield (determined from the TCSPC data as above) varied from 0.97 for the electrolyte with the highest Lewis acidity (0.1 M $Li^+$, 0 M tBP) to 0.7 for the most "basic" electrolyte (0 M $Li^+$, 0.5 M tBP), indicating, depending on the electrolyte employed, substantial (up to 30%) losses of photocurrent generation due to excited-state decay to ground. Figure 5(ii) shows a plot of injection yield versus device photocurrent, demonstrating that a linear correlation is observed, strongly indicative of electron injection losses being a key determinant of device photocurrent efficiency, as is discussed in more detail below.

(51) Nazeeruddin, M. K.; Kay, A.; Rodicio, I.; Humphrybaker, R.; Muller, E.; Liska, P.; Vlachopoulos, N.; Grätzel, M. *J. Am. Chem. Soc.* **1993**, *115*, 6382–6390.
(52) Boschloo, G.; Haggman, L.; Hagfeldt, A. *J. Phys. Chem. B* **2006**, *110*, 13144–13150.
(53) Kato, T.; Fujimoto, M.; Kado, T.; Sakaguchi, S.; Kosugi, D.; Shiratuchi, R.; Takashima, W.; Kaneto, K.; Hayase, S. *J. Electrochem. Soc.* **2005**, *152*, A1105−A1108.
(54) Boschloo, G.; Lindstrom, J.; Magnusson, E.; Holmberg, A.; Hagfeldt, A. *J. Photochem. Photobiol. A: Chemistry* **2002**, *148*, 11–15.
(55) O'Regan, B. C.; Scully, S.; Mayer, A. C.; Palomares, E.; Durrant, J. *J. Phys. Chem. B* **2005**, *109*, 4616–4623.

## Discussion

In this paper we have employed time-resolved single photon counting to investigate the influence of a range of parameters upon the kinetics of electron injection in N719-sensitized solar cells. The injection half-time we obtain for a solar cell employing a "standard" electrolyte (0.1 M $Li^+$, 0.5 M tBP), $t_{50\%}$ = 200 ps, is found to be in good agreement with our previous studies of electron dynamics by ultrafast pump/probe transient absorption spectroscopy.[8] The emission decay dynamics in this standard cell (and indeed in all $TiO_2$ samples studied) were found to be well represented by convoluting stretched exponential functions with the instrument response function. This is in good agreement with our previously proposed model for electron injection in which the observed stretched exponential dynamics were shown to be consistent with local inhomogeneities in the $TiO_2$ CB energy.[37]

**Energy Dependence of Injection Kinetics.** The primary determinant of electron injection kinetics in the studies we report herein is found to be the composition of the redox electrolyte, and specifically the concentrations of the additives $Li^+$ and tBP in this electrolyte. The injection half-time was observed to change from <60 ps for 0.1 M $Li^+$/0 M tBP to ~550 ps for 0 M $Li^+$/0.5 M tBP. This dependence was correlated with the influence of these additives upon the relative energetics of $TiO_2$ CB determined from charge extraction data. High charge density cations, such as $Li^+$, have been shown to be "potential-determining ions", adsorbing to and/or intercalating into the nanocrystalline $TiO_2$ film, and thereby modulating the film charge and thus the film energetics. The addition of 0.1 M $Li^+$ has been shown to induce a >1 V downward shift in the CB energy of unsensitized $TiO_2$ films and a 300 meV shift in N3/$TiO_2$ films.[23,56] Conversely, the addition of tBP has been shown to raise the energy of the $TiO_2$ CB, attributed to its Lewis base characteristics, either by direct coordination to the $TiO_2$ surface via lone pairs on the N moiety[57,58] or through reducing the surface-adsorbed proton concentration, as illustrated in Scheme 3.[50]

The correlation between injection half-time and the conduction band energetics shown in Figure 5(i) indicates that a 280 meV shift in CB energy results in an ~8 fold retardation of the injection kinetics. This correlation is in agreement with our previous analysis of injection kinetics in N3-sensitized $TiO_2$ films in three-electrode photoelectrochemical cells by ultrafast transient absorption spectroscopy, where the addition of 0.1 M $Li^+$ ions was observed to result in a 7-fold acceleration of injection kinetics, correlated with a 300 meV shift in $TiO_2$ CB energetics.[23] We further note that we have observed a quantitatively similar dependence of injection kinetics upon the relative energetics of the dye excited state relative to the $TiO_2$ CB (referred to hereafter as $\Delta E_{inj}^{rel}$) in studies of porphyrin-sensitized $TiO_2$ films as a function of porphyrin singlet energy, where a 300 meV shift in singlet energy resulted in an order of magnitude acceleration of injection kinetics, as we report in detail elsewhere.[59]

The dependence of injection half-time upon the energetics of electron injection, $\Delta E_{inj}^{rel}$, can be analyzed in terms of changes in the influence of $\Delta E_{inj}^{rel}$ upon the density of energetically accessible $TiO_2$ acceptor states. Previous studies have indicated that the effective density of states in the $TiO_2$ CB can be considered to increase exponentially with energy, $g(E) \propto \exp(E/E_0)$,[48] as illustrated in Figure 5, with values for $E_0$ typically of the order 100 meV.[48] Assuming, as we have proposed previously,[48] that the rate constant for electron injection is proportional to the number of accessible states, we conclude that $t_{50\%} \propto \exp(-E/E_0)$. Following this relationship, a 280 meV increase in $\Delta E_{inj}^{rel}$ can be expected to result in an acceleration of the injection half-time by ~16, in reasonable agreement with the observed acceleration (~8-fold). We thus conclude that the observed dependence of $t_{50\%}$ upon $TiO_2$ CB energy is in good quantitative agreement with a simple model in which the rate of electron injection is proportional to the density of energetically accessible acceptor states.

We note that this model does not distinguish between "trap" and "conduction band" states, but only considers a simple, exponentially increasing density of states. This assumption is consistent with experimental observations that the density of electrons in such $TiO_2$ films increases exponentially with applied negative biases over a wide potential range. We further note that this analysis is independent of whether one considers the relevant density of states determining electron injection to be the magnitude of $g(E)$ at the dye excited state oxidation energy $E_m(S^+/S^*)$ or at an energy corresponding to $E_m(S^+/S^*) - \lambda$, where $\lambda$ is the reorganization energy (corresponding, according to Marcus−Gerischer, to the energy for activationless electron injection), or integration of the density of states up to either of these energies, as in all cases an exponential density of states will give the same relative change in injection dynamics for a given change in $\Delta E_{inj}^{rel}$. It should be noted that this analysis considers only the effect of $Li^+$ and tBP concentrations upon the relative energetics of the $TiO_2$ CB versus the dye excited state, and not other effects specific to either $Li^+$ or tBP (for example, deriving from surface binding of tBP). A more detailed analysis, in which the influence of tBP and $Li^+$ ions will be analyzed independently, will be presented elsewhere. We finally note that this model, assuming an exponential density of states but with local inhomogeneities in the magnitude of $\Delta E_{inj}^{rel}$,[37] has been shown to be in good agreement with the stretched-exponential injection dynamics reported herein.

**Singlet versus Triplet Injection.** The analysis we have reported herein focuses on electron injection on the picosecond time scale, and therefore is assigned to electron injection from the N719 triplet state formed by ultrafast (~100 fs) intersystem crossing from the initially generated singlet excited state, as illustrated in Scheme 5. We have previously invoked a change from singlet to triplet injection to explain the increase in photocurrent from $RuL_3$ (L = 4,4′-dicarboxy-2,2′-bipyridyl)-sensitized $TiO_2$ in an ethanol electrolyte as the band edge was shifted down by the addition of acid to the electrolyte.[60] The dependence of injection kinetics upon the relative energetics of the dye excited state versus the $TiO_2$ CB, $\Delta E_{inj}^{rel}$, found herein allows us to analyze further the relative injection dynamics from the N719 singlet and triplet excited states. The N719 singlet and triplet excited state energies can be estimated from steady-state absorption and emission data to be approximately 1.95 and 1.6 eV, respectively. Employing the dependence of injection half-time upon $\Delta E_{inj}^{rel}$ found herein, we conclude that the rate constant for electron injection from the singlet excited state

(56) Redmond, G.; Fitzmaurice, D. *J. Phys. Chem.* **1993**, *97*, 1426–1430.
(57) Xiong, B. T.; Zhou, B. X.; Zhu, Z. Y.; Gao, T.; Li, L. H.; Cai, J.; Cai, W. M. *Chin. J. Chem.* **2008**, *26*, 70–76.
(58) Kusama, H.; Orita, H.; Sugihara, H. *Solar Energy Mater. Solar Cells* **2008**, *92*, 84–87.
(59) Dos Santos, T.; Durrant, J. R.; Moser, A.; Officer, D. Manuscript in preparation.
(60) O'Regan, B. University of Washington, 1998.

***Scheme 5.*** Energetics and Kinetics of Electron Injection in a "Standard" DSSC, Focusing in Particular upon Comparison of Triplet versus Singlet Injection[a]

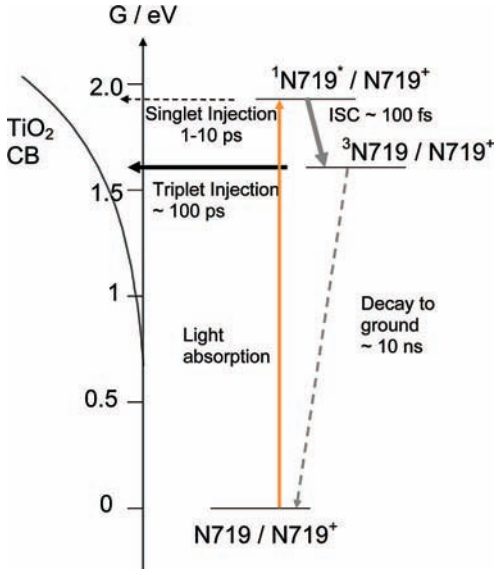


[a] Energies are given as free energies relative to the dye ground state. The energy difference, $\Delta E_{inj}^{rel}$, referred to in the Discussion refers to the energy difference between the dye excited states and the density of acceptor states in the $TiO_2$. Given the exponential shape of this density of states, assigned to the $TiO_2$ CB/trap states, and thus the difficulty of defining an absolute CB "edge", we consider herein only the effect of variations in the relative value of this energy difference, rather than its absolute value.

should be ~1 order of magnitude faster than from the triplet state. This difference in injection rates is consistent with previous analyses of biphasic injection dynamics for N3-sensitized $TiO_2$ films,[15,61] assigned to parallel pathways for electron injection from the N3 singlet and triplet states. However, this 1 order of magnitude difference in injection rate constant is much smaller than the difference in the kinetics of the competing decay pathways from these states, this being ~100 fs for the singlet state and ~10 ns for the triplet state, resulting in it being much easier to achieve efficient electron injection from the triplet rather than the singlet state of the N719 dye.

The analysis detailed above indicates that electron injection from the singlet excited state of ruthenium bipyridyl dyes is only likely to be observed for very favorable interfacial energetics (i.e., very large $\Delta E_{inj}^{rel}$), such as those present for N3-sensitized $TiO_2$ films in the absence of other potential-determining species (due to the acidic properties of N3). For more modest values of $\Delta E_{inj}^{rel}$, such as those observed in typical devices due to the presence of the potential-determining electrolyte, singlet injection does not compete effectively with intersystem crossing to the triplet state. Intersystem crossing to the triplet state results in a loss of $\Delta E_{inj}^{rel}$ (due to the ~300 meV lower energy of this triplet state), and thus ~10-fold retardation of the injection kinetics. However, this retardation is outweighed by the 5 orders of magnitude increase in excited state lifetime, enabling electron injection to proceed from this triplet state with a high quantum efficiency. As a consequence, except for very large values of $\Delta E_{inj}^{rel}$, electron injection in N719-sensitized $TiO_2$ films and devices is likely to be dominated by injection from the N719 triplet state, consistent with the data we report herein. We note that conditions resulting in a large value of $\Delta E_{inj}^{rel}$, and thus significant injection from the singlet state, would necessarily result in a large free energy loss associated with the electron injection, and are therefore not likely to be compatible with efficient overall device performance.

**Other Materials Factors Influencing Electron Injection Kinetics.** In addition to the influence of $Li^+$ and tBP concentration in the electrolyte upon the injection kinetics, we also investigated the dependence of the injection kinetics upon the $TiO_2$ preparation methodology, the presence of a redox couple in the electrolyte, and N719 dye loading. In all these cases, no significant variation of injection kinetics could be resolved. It can thus be concluded that the primary device composition factor determining the kinetics of electron injection for N719-sensitized $TiO_2$ solar cells is indeed the concentration of potential-determining ions in the solution.

Considering the dependence upon film preparation, the sensitivity of electron injection rates to sample preparation, and particularly to film crystallinity, has been previously highlighted.[44] In this paper, we studied two extreme cases of film fabrication, employing either acid or base peptization, which might be expected to influence the film surface charge, and therefore $\Delta E_{inj}^{rel}$. However, the absence of any change in injection kinetics strongly indicates that the energetics of electron injection, $\Delta E_{inj}^{rel}$, in the complete devices were independent of the peptization employed. This can most probably be attributed to the subsequent film treatments (sintering, dye sensitization, and electrolyte addition) removing any initial difference in energetics deriving from the peptization. We note that we have previously shown that the kinetics of charge recombination, and indeed overall device performance, are dependent upon the peptization step employed. [45] At present the origin of the different dependence of electron injection and recombination upon film peptization is unclear, although we note that the recombination dynamics have been suggested to be particularly sensitive to intraband recombination sites on the film surface, which in turn may be sensitive to the peptization procedure.

Several reports have reported both reductive quenching of Ru-bipyridyl excited states by iodide[41,42] and oxidative quenching by iodine[43] and considered the potential impact of these quenching pathways upon device performance. We find herein that the transient emission dynamics observed for both the N719/$TiO_2$ DSSCs and the N719/$ZrO_2$ control films were independent of the presence of the iodide/iodine redox couple in the electrolyte, at least at the concentrations studied (0.7 M iodide, 0.1 M iodine). We note this observation contrasts with that of a recent study by Smeigh et al.[40] We conclude that neither oxidative nor reductive quenching of the N719 excited states by the redox couple is a significant decay pathway for the devices studied herein, consistent with the observed efficient device operation.

Previous studies have discussed the potential importance of dye aggregation upon the observed injection dynamics.[31] We note that, in the studies reported herein, the sensitizing solution was sonicated prior to sensitization to break up any such dye aggregates. We further note we obtained similar injection data for a broad range of dye loadings, suggesting that any dye aggregation induced by high dye loadings did not significantly impact upon the observed data. In any case, the high device internal photocurrent quantum efficiencies (~86%) in electrolyte A strongly indicates that dye aggregation did not have a significant impact upon the data reported herein.

**Injection Dynamics under Applied Bias.** We consider next the effect of applying negative bias to our standard N719/$TiO_2$

(61) Tachibana, Y.; Moser, J. E.; Grätzel, M.; Klug, D. R.; Durrant, J. R. *J. Phys. Chem.* **1996**, *100*, 20056–20062.

DSSCs. As shown in Figure 3, we observe only a relatively small dependence of $t_{50\%}$ and $\phi_{inj}$ on applied bias, with the dark application of −1070 mV causing an increase in $t_{50\%}$ from 180 ± 45 to 230 ± 60 ps and a corresponding 8% decrease in $\phi_{inj}$ from 0.83 ± 0.04 to 0.76 ± 0.04. Given this potential range results in a variation of electron density and $TiO_2$ Fermi level significantly larger than that generated by typical device operation under AM1.5 irradiation, this observation strongly suggests that the electron injection yield for such N719-sensitized DSSCs is relatively insensitive to electron density in the $TiO_2$ film over the operating range of the device. This is consistent with the relatively low electron densities injected into the $TiO_2$ film ($\sim 10^{18}$ $cm^{-3}$, corresponding to up to ~10 electrons per nanoparticle), with the high $TiO_2$ dielectric constant resulting in negligible electron/electron repulsion. We further note that the absence of a strong bias dependence of the emission dynamics indicates that thermal excitation of injected electrons back to the dye lowest unoccupied molecular orbitals, resulting in repopulation of the dye excited state, does not appear to be a key limiting factor for device operation. This contrasts, for example, to charge separation in photosynthetic reaction centers, where thermal repopulation of singlet excited states results in the observation of "delayed fluorescence".

The relatively modest bias dependence we observe herein can most probably be assigned to a reduction in the density of unoccupied acceptor states, as we have discussed previously in analogous model system studies.[62] The observed modest bias dependence may result in a small decrease in device fill factor and open circuit voltage. However, we note that a significant bias dependence was only observed for the highest applied voltages (>0.8 V), with our data indicating a loss of injection yield due the increase of electron density of ≤2% under the range of typical device operation, indicating that this bias-dependent loss of injection yield does not significantly impact upon the photovoltaic performance of the DSSCs studied herein.

**Correlation between Injection Kinetics and Device Performance.** We have concluded that the primary factor determining the efficiency of electron injection for the N719-sensitized DSSCs studied herein is the energy of the density of $TiO_2$ acceptor states relative to the dye excited state, $\Delta E_{inj}^{rel}$, and that this energy difference is primarily determined by the concentration of additives such as $Li^+$ and tBP in the electrolyte (or alternatives such as guanadinium thiocyanate).[49,63] We find that, when we vary the concentration of these additives, there is good correlation between the efficiency of electron injection, determined by our transient emission studies, and device short circuit current $J_{sc}$. We note that these studies have employed thin (4 $\mu$m) $TiO_2$ films, thereby minimizing recombination losses during electron transport to, and collection by, the FTO electrode. A more detailed analysis of this dependence, including consideration of the influence of additive concentration upon the efficiency of electron collection as well as electron injection, is reported elsewhere.[39] Notwithstanding this consideration, the data report herein show a variation of injection efficiency between 0.7 and 0.97 for the range of additive concentrations studied, and strongly indicate that variations in electron injection efficiency are a key determinant of the variations in short circuit current density as a function of electrolyte composition.

A particularly striking observation from the results reported herein is that the electrolyte additive concentrations resulting in optimum overall device efficiency do not correspond to those yielding the fastest, and therefore most efficient, electron injection. The fastest electron injection dynamics, observed in the presence of 0.1 M $Li^+$ and 0 M tBP, yielded an injection efficiency of 97%, and the largest device $J_{sc}$. However, in this case, the device open circuit voltage is only 565 mV, attributed to the relatively low energy of the $TiO_2$ acceptor states. Under these conditions, electron injection results in a relatively large loss of free energy. Optimum device performance is obtained with the addition of 0.5 M tBP, raising the energy of the $TiO_2$ density of acceptor states by ~200 meV. This reduces the injection efficiency by ~10%, correlated with a loss of device photocurrent. However, this loss of photocurrent is more than compensated for by an increase in the $TiO_2$ Fermi level at which the interfacial recombination flux matches the photogeneration flux, resulting in a 100 mV increase in $V_{OC}$ and higher overall device efficiency.

This influence of electron injection upon device efficiency can be readily understood in terms of the "minimization of kinetic redundancy", as we have proposed previously.[8] Efficient device performance requires only that electron injection is fast relative to excited state decay to ground, as we discussed previously in terms of phthalocyanine sensitizer dyes.[64] Optimum device performance is a compromise between achieving a sufficiently large energetic driving force for electron injection (i.e., $\Delta E_{inj}^{rel}$) to enable electron injection to compete with excited state to ground and raising the $TiO_2$ CB as high as possible to minimize recombination losses and thus raise cell voltage. It can be viewed as a requirement to minimize the free energy loss associated with electron injection, while still maintaining a reasonably high quantum efficiency for this process.

We have recently reported that charge separation in polymer/fullerene solar cells may require a relatively large energetic driving force (or polymer/fullerene LUMO level offset).[65] This requirement comes from the relatively low dielectric constant of such organic materials, resulting in relatively strong Coulomb attraction of electrons and holes and causing geminate recombination losses to become a significant loss pathway in such devices. This situation can be contrasted with the electron injection dynamics we report here for DSSCs. In these devices, the relatively high dielectric constant of the $TiO_2$ and the high ionic strength of the electrolyte result in relatively weak Coulomb attraction of injected electrons with dye cations. As such, geminate recombination does not appear to be a significant factor in DSSCs. In these devices, the efficiency of charge separation is determined only by the relative kinetics of electron injection versus excited state decay to ground.

**Concluding Remarks.** We conclude that, even for N719-sensitized $TiO_2$-based DSSCs, the most widely studied device materials to date, electron injection is a key limitation upon device performance. Efficient electron injection requires that electron injection is fast relative to excited state decay to ground. As such, it is dependent upon excited state lifetime; for example, the relatively short singlet excited lifetime of N719 (~100 fs) relative to its corresponding triplet state (~10 ns) results in triplet

(62) Oregan, B.; Moser, J.; Anderson, M.; Grätzel, M. *J. Phys. Chem.* **1990**, *94*, 8720–8726.
(63) Lee, K. M.; Suryanarayanan, V.; Ho, K. C.; Thomas, K. R. J.; Lin, J. T. *Solar Energy Mater. Solar Cells* **2007**, *91*, 1426–1431.
(64) Morandeira, A.; Lopez-Duarte, I.; Martinez-Diaz, M. V.; O' Regan, B.; Shuttle, C.; Haji-Zainulabidin, N. A.; Torres, T.; Palomares, E.; Durrant, J. R. *J. Am. Chem. Soc.* **2007**, *129*, 9250–9250.
(65) Ohkita, H.; Cook, S.; Astuti, Y.; Duffy, W.; Tierney, S.; Zhang, W.; Heeney, M.; McCulloch, I.; Nelson, J.; Bradley, D. D. C.; Durrant, J. R. *J. Am. Chem. Soc.* **2008**, *130*, 3030–3042.

state injection being the optimum pathway for charge separation in efficient devices. The kinetics of electron injection are strongly dependent upon the relative energetics of the dye excited state relative to unoccupied $TiO_2$ acceptor states, and therefore to the influence of "potential-determining" additives in the electrolyte on the interfacial charge densities/dipoles. Optimum device performance requires optimization of these additive concentrations such as to allow reasonably efficient electron injection while at the same time minimizing the recombination flux at a given film Fermi level, and thereby maximizing cell voltage. For the device series studied herein, this optimum device performance is found to correspond to additive concentrations yielding an injection half-time of ~200 ps and an injection quantum yield of ~84%.

**Acknowledgment.** The authors thank the EPSRC Supergen and Materials for Energy programmes, and EU programme Robust DSC, for funding, Li Xiaoe for technical assistance, and Ana Morandeira for helpful discussions.

JA8091278